Secondary Nucleation in a Class II System: Ammonium Sulfate-Water

GORDON R. YOUNGQUIST and ALAN D. RANDOLPH

Department of Chemical Engineering
University of Arizona, Tucson, Arizona 85721

Secondary nucleation at low supersaturation for the ammonium sulfate-water system was studied using a seeded continuous crystallizer. Counter size distribution measurements in the subsieve size range indicated that nuclei are formed by microattrition of seed crystals and that the growth rate of the nuclei is very small. Nucleation rate was correlated with the characteristics of the secondary environment. The results of this correlation, which shows strong dependence on stirring rate and essentially linear dependence on solids concentration, indicate that secondary nuclei are generated by collisions of the seed crystals with the impeller blades.

Nucleation of crystals may be homogeneous, heterogeneous, or secondary. Homogeneous nucleation occurs from clear, highly supersaturated solutions when aggregates of solute molecules attain sufficient order and size to form a stable, solid particle. Heterogeneous nucleation occurs when the formation of such aggregates is catalyzed by foreign particles. Secondary nucleation occurs when nucleation is induced by the presence of crystalline solute or "seed" crystals. In most cases of industrial interest, for example, the production of crystals from batch or continuous crystallizers, secondary nucleation is dominant. Hence, much recent effort has been devoted to determining the mechanisms and kinetics of secondary nucleation.

Several investigations have provided insight into these mechanisms. Mason and Strickland-Constable (7) have suggested that three types of nucleation occur in the presence of seeds. The first is initial breeding which results when dry seeds are placed in solution and microscopic crystal dust washes off the dry seeds to form nuclei. The second is needle breeding resulting from the breakage of large dendritic growths. The third is collision breeding in which nucleation is induced by collisions of seed crystals with solid surfaces. Of these, only the last is a major source of secondary nuclei in well-designed crystallizers. Clearly the first is a seeding effect and the second is gross breakage of dendritic seed crystals. Such dendritic growth is minimized in well-designed crystallizers operating with low supersaturation. Lal et al. (5) were perhaps the first to demonstrate conclusively the existence of collision breeding. Using $MgSO_4 \cdot 7H_2O$, KCl, and KBr crystals, they showed that fluid shear alone does not give rise to nucleation when a cured seed crystal is placed in supersaturated solution. Crystal-solid contacts, however, did produce nuclei. In a classic study, Clontz and McCabe (2) measured the number of nuclei resulting from the impact of a glass rod on a face of a $MgSO_4 \cdot 7H_2O$ crystal. They showed the number of nuclei produced per unit crystal area to be approximately linear with impact energy and with supersaturation. Crystal-crystal contacts produced two to five times as many nuclei as did crystal-rod contacts. Johnson, Rousseau, and McCabe (4) extended this work to show that surface roughness and hardness of the crystal face as well as the hardness of the contacting surface affect the number of nuclei produced.

These studies have shown that secondary nucleation is predominantly due to collision breeding. That is, nuclei result from the collision of seed crystals with solid surfaces, which in the case of a stirred crystallizer may be other crystals, impeller blades, or crystallizer surfaces. They do not, however, provide kinetic information useful for predicting or correlating nucleation rates except to suggest which operating variables may be important. There have been relatively few definitive kinetic studies. No fundamental theory for prediction or correlation of secondary nucleation rates exists. Most experimental data have been obtained using MSMPR crystallizers. These data frequently have been correlated empirically using power law models of the form $B^0 = k_n S^i M_T^j$ where B^0 is nucleation rate, S is supersaturation, and M_T is the solids concentration of the slurry. The data of Timm and Larson (13), Larson et al. (6) and Rosen and Hulburt (11) are typical.

Thus, most studies of secondary nucleation have been either qualitative, aimed at elucidating the mechanisms by which this type of nucleation occurs, or quantitative, aimed broadly at describing the kinetics of the process by empirical means. Rarely have the two been combined, a notable exception being the work of Randolph and Cise (1, 9). In this paper, both mechanistic and kinetic aspects of the secondary nucleation of ammonium sulfate in a seeded continuous crystallizer are described. Population densities measured in the subsieve size range indicated that under the experimental conditions birth rather than growth populates the crystal size distribution in this size range. Secondary nucleation is thus observed directly. Nucleation rates were correlated with the characteristics of the secondary environment.

EXPERIMENT

The apparatus and general procedures used in this study have been described in detail elsewhere by Cise and Randolph (1). The crystallizer is of the continuous mixed suspension

Correspondence concerning this paper should be addressed to A. D. Randolph. G. R. Youngquist is with Clarkson College of Technology, Potsdam, New York 13676.

type with the key feature of mixed removal of product fines coupled with total retention of larger seed crystals. This is accomplished by discharging the product stream through a 200 mesh stainless steel screen. The size distribution of product fines generated by secondary nucleation and leaving the crystallizer was determined using a Model "T" Coulter Counter. Use of a 70 micron aperture sampling probe allowed measurement of the size distribution in the range 1.26 to 25.4 microns.

Seed crystals were obtained by screening Baker reagent grade anhydrous ammonium sulfate into narrow size fractions. Fifteen to 25 grams of seeds of 3 sizes ($-70 + 80$, $-45 + 50$, and $-25 + 30$ mesh) were used in the various runs.

In making a run, filtered ammonium sulfate solution saturated at a temperature 0.5° to 2.0°C. above the crystallizer temperature was fed at a predetermined rate to give residence times of approximately 5 to 16 minutes. A measured quantity of seeds of known size was then introduced ($t = 0$) to the crystallizer and sampling of the effluent with the counter was begun. Size determinations were made at roughly 10 min. intervals. Three agitation rates were investigated: 545, 610, and 675 rev./min. In most runs, step changes in stirrer rev./min. were made and the response followed for 5 to 10 residence times. In order to characterize the seeds during a run, small samples of slurry were pipetted from the crystallizer at various times and photomicrographed. The mass of seeds withdrawn was negligible compared to the total seed mass. The average seed size was calculated as the geometric mean of the two longest dimensions measured from the photographs. At the end of the run, the entire seed slurry was dropped from the crystallizer into a large Buchner funnel and rapidly filtered. The seeds then were carefully dried, weighed, and subjected to screen analysis.

EXPERIMENTAL OBSERVATIONS AND RESULTS

Since strong supersaturation dependence of nucleation rate in the ammonium sulfate-water system has often been alluded to (*10, 12*), some preliminary tests were conducted using the crystallizer to determine what supersaturation levels could be sustained in the absence of seeds without inducing homogeneous nucleation. These showed that no nucleation occurred in stirred unseeded solutions that were subcooled up to 2.7°C. Greater subcooling resulted in an enormous shower of nuclei which grew very rapidly. All subsequent runs were made with a temperature difference between saturator and crystallizer of 2°C. or less in order to avoid the interfering effects of this homogeneous nucleation.

In the initial runs, the crystallizer was seeded with 1 to 5 g. of seeds. With these quantities, an effect similar to the homogeneous nucleation described above was noted. That is, a shower of nuclei was induced, and these nuclei grew very rapidly to a size which prevented passage through the retaining screen in the discharge. To illustrate, when the crystallizer was seeded with 5 g. of $-25 +30$ mesh seeds and with a temperature difference between saturator and crystallizer of 2.0°C., a shower of nuclei was noted immediately. The population of these new crystals was so great that it was impossible to determine the product fines size distribution with the Counter because of plugging of the aperture of the sampling probe. The run was allowed to continue for approximately 3 hours. Screen analysis of the crystals in the crystallizer at the end of the run showed a very broad distribution of sizes, with 67% by weight of size less than that of the original seeds. By contrast, when the initial seed mass was 15 g. or more, these effects were not observed. No shower of nuclei was induced, and the seed size distribution at the end of the run was quite narrow with negligible amounts less than the original seed size. This suggests that the mechanism of secondary nucleation may be different at high supersaturations from that at low supersaturations, or, more likely, the metastable limit for the occurance of homogeneous nucleation is lowered in the presence of seed. It is a moot question whether these nuclei result from a "homogeneous" or "secondary" mechanism; homogeneous supersaturation driving forces play an important role in their formation, yet their occurence is stimulated by seed crystals. In order to operate the crystallizer at low stable levels of supersaturation where the seed mass could be well characterized, it was necessary to introduce large quantities of seeds initially.

CLASS II BEHAVIOR

The behavior noted upon seeding is due to the fact that ammonium sulfate-water is inherently a Class II system. Class II systems are high yield systems such that the supersaturation level for stable operation of the crystallizer is very low, approaching zero. Thus, when small quantities of seeds are introduced the surface area of these initial seeds is insufficient to reduce the supersaturation to a stable low level by growth of the seeds. Large numbers of nuclei which grow very rapidly are induced, adding to the seed population until stable low supersaturation conditions are achieved. On the other hand, when large quantities of seeds are introduced, the surface area of the initial magma is sufficient to immediately reduce the supersaturation to stable levels. No nucleation then occurs beyond the secondary nucleation characteristic of these stable conditions. These observations support the existence of a metastable limit for supersaturation beyond which homogeneous nucleation occurs in the presence of a seed bed. It should be emphasized, however, that the observations to be presented regarding the kinetics and mechanism of secondary nucleation of ammonium sulfate are valid only at the low supersaturation levels where meaningful measurements could be made and are not useful for predicting instabilities which may arise under other conditions.

The production rate for a continuous crystallizer is given by

$$P = Q(C_f - C) \tag{1}$$

For a Class II system, the effluent concentration C is essentially the saturation value at the operating temperature of the crystallizer. Hence,

$$P = Q(C_f - C_s) \tag{2}$$

As operated under stable conditions in this study, the depletion of solute from the feed stream is essentially due to growth of the seeds introduced initially and retained in the crystallizer. Thus

$$P = \frac{dW}{dt} = Q(C_f - C_s) \tag{3}$$

and for constant conditions

$$W_t - W_i = Q(C_f - C_s)t \tag{4}$$

For small temperature ranges

$$C_f - C_s = k(T_f - T) \tag{5}$$

so that Equation (4) becomes

$$W_t - W_i = kQ(T_f - T)t \tag{6}$$

This relationship was shown to be valid using the seed mass at the end of the run as W_t and the length of the run as t. The excellent agreement of the data with Equation (6) is shown in Figure 1. These data contain two

points, shown as squares, where the initial seed mass was small and nuclei showers were induced. The fact that these also agree with Equation (6) demonstrates that the system spontaneously adjusts to Class II behavior.

EVALUATION AND CORRELATION OF NUCLEATION RATES

Data obtained during a typical run are shown in the population density time plot of Figure 2. The population density at the smallest sizes is very high initially due to initial breeding. Ammonium sulfate "dust" at the surface of the initially dry seeds washes off upon introduction to the crystallizer. The population density subsequently decays (due to washout of these initial breeds) to a level representative of true secondary nucleation.

Since the seed crystals are totally retained, true steady-state operation of the crystallizer can never be achieved. The seeds are continually increasing in size due to growth and the supersaturation level, though very small decreases as the seed area becomes larger. Examining Figure 2, however, it is apparent that a quasi-steady state is achieved in which the population density changes very slowly with time. This was typical of all the runs made. The two steps in the population density-time curves resulted from step changes in stirrer rev./min. The response to these changes was very rapid, and steady new population levels were achieved in but a few minutes.

Most analyses of crystallizer data are based on the population balance, one form of which (8) is

$$\frac{\partial n}{\partial t} + \frac{\partial (Gn)}{\partial L} + \frac{n\, d(\log V_T)}{dt} = \sum_i \frac{n_i Q_i}{V} + B(L) - D(L) \quad (7)$$

This complex relationship may be simplified somewhat by invoking the conditions of the present experiments, a. constant slurry volume, b. clear liquor feed, and c. perfect mixing, with the result

$$\frac{\partial n}{\partial t} + \frac{\partial (Gn)}{\partial L} = -\frac{n}{\tau} + B(L) - D(L) \quad (8)$$

Further, the quasi-steady state nature of the data indicates

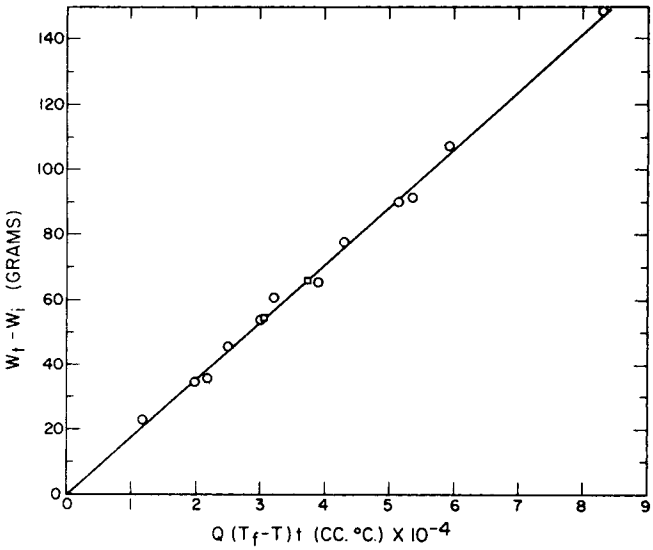

Fig. 1. Class II behavior of ammonium sulfate-water.

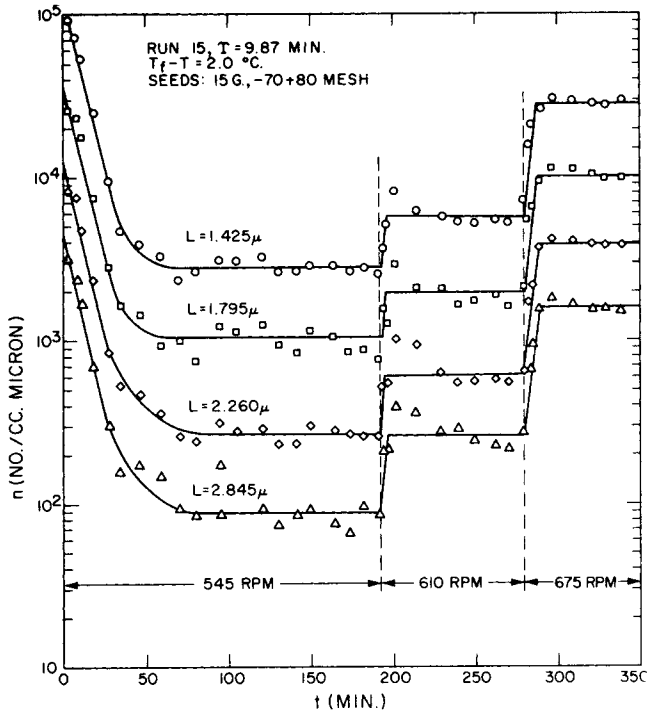

Fig. 2. Population density data for a typical run.

that $\partial n/\partial t$ is negligible. If the birth function $B(L)$ and death function $D(L)$ may also be neglected, the usual MSMPR equation results. That is, at any time

$$\frac{d(Gn)}{dL} = -\frac{n}{\tau} \quad (9)$$

Assuming McCabe's ΔL law, $G \neq G(L)$, Equation (9) may be integrated directly to give

$$n = n^0 \exp\left[-\frac{L}{G\tau}\right] \quad (10)$$

In a typical MSMPR analysis, log n is plotted versus L and the kinetic parameters n^0 and G are obtained from the intercept and slope, respectively. The nucleation rate is then calculated as

$$B^0 = n^0 G \quad (11)$$

This assumes that all new crystals (nuclei) are formed only at size zero and that larger sizes are populated by growth alone.

Figure 3 shows some typical size distributions given by the population densities at one time during a run. Clearly, log n versus L is not linear, indicating that one or more of the assumptions leading to Equation (10) is invalid. The simplifications of Equation (7) due to experimental conditions were all verified independently and are above suspicion. This leaves the validity of assumptions of constant growth rate and negligible birth and death functions to be considered. Consider first the assumption of constant growth rate. If $G = G(L)$, Equation (9) may be expanded to give

$$n\frac{\partial G}{\partial L} + G\frac{\partial n}{\partial L} = -\frac{n}{t} \quad (12)$$

or rearranging

$$\frac{\partial \log n}{\partial L} = -\frac{1/\tau + \dfrac{\partial G}{\partial L}}{G} \quad (13)$$

It should be apparent from Equation (13) that if G increases greatly with increasing size, then a plot of ln n versus L would have a characteristic shape similar to that of the data shown in Figure 3. This type of size dependence for growth rate is unusual. If growth was influenced by mass transfer effects, decreasing growth rate with increasing size is to be expected and if surface kinetics alone are involved, growth rate should be independent of size. However, recent work by Wey and Estrin (14) which takes into account the variation of solubility with particle size indicates that the growth of small particles may indeed be a strongly increasing function of size. In spite of this, several features of the experimental data indicate rather convincingly that the size distribution is *not* populated by growth but rather by birth in the size ranges measured. These are as follows:

1. For a given run, the shape of the size distribution at constant rev./min. was independent of time. Growth rate is normally found to be at least linear with supersaturation. Supersaturation in the crystallizer continually decreases with time due to increased area of the seeds and hence the growth rate should decrease. As determined by photographic measurement, the growth rate of the seed crystals decreased, in some cases by as much as a factor of two. Thus, if growth populated the size distribution, the shape of the distribution should change with supersaturation (thus growth rate) consistent with Equation 13.

2. For different runs at constant rev./min., holding time, and initial seed size and mass but with different values of $T_f - T$ (thus supersaturation) the shape of the size distribution is essentially the same as shown by Figure 3. The magnitude of the population density is different, however. Again, if the size distribution is populated by growth, different supersaturations should lead to different shapes for the distributions.

3. The response of the population densities for *all* sizes to step changes in stirrer rev./min. was virtually instantaneous. This certainly would not be expected if growth populated the distributions. Rather, a distinct time lag corresponding to the time required for growth from essentially zero size to the measured sizes would be expected. This time lag would be considerable, since the data indicate at best a very small growth rate for small sizes.

4. Photographs of the seed crystals withdrawn during the course of a run give strong visual evidence of collision breeding by attrition. The sequence of photographs in Figure 4 is very illustrative. Cracks and chips at the edges and corners of even relatively small seeds are evident. These became more pronounced with increasing size and at high stirring rates, and the seed ends in some cases became quite rounded.

As a result of these observations, it was concluded that the measured size distributions were populated principally by collision breeding. That is, impacts of the seed crystals with the stirrer blades, crystallizer surfaces, and other crystals produced crystal fragments (nuclei) in the size range measured. The growth rate of these fragments is sufficiently small that birth is balanced by washout. The birth function $B(L)$ and washout terms are, therefore, large relative to the growth term in the population balance and Equation (8) is reduced to

$$B(L) = \frac{n}{\tau} \tag{14}$$

The death term has been neglected since no gross attrition is likely at the very small sizes of the secondary nuclei. The nucleation rate is then given by:

$$B^0 = \int_{a_0}^{a_1} B(L)dL = \frac{1}{\tau}\int_{a_0}^{a_1} ndL \tag{15}$$

Equations (14) and (15) represent maximum estimates of the birth distribution and nucleation rate since the population flux due to growth is entirely suppressed.

In order to determine the nucleation rate, the integral of Equation (15) must be evaluated from the experimental size distributions. This presents a dilemma. The population density was measured in the size range 1.26 to 25.4 microns. In this range $B(L)$ monotonically decreases with size, being very large at small sizes and rapidly decreasing to essentially zero. Figure 5 is typical. Thus, the major contribution to the integral occurs at small L. The lower integration limit a_0 should be the critical nucleus size. In the absence of experimental data at very small sizes, four different methods of estimating the nucleation rate from the existing experimental data were examined. Each involved fitting the experimental $B(L)$ data as calculated from Equation (14) to a prescribed analytical form. These $B(L)$ data were then used to obtain the nucleation rate from Equation (15). The methods are as follows:

1. $B(L)$ was fit, using least squares, to

$$B(L) = bL^m \tag{16}$$

This function was suggested by the fact that log-log plots of the experimental size distributions were essentially linear, especially in the small size range. In determining the nucleation rate from Equation (15), the birth function was taken as

$$\begin{aligned} B(L) &= 0, \qquad L < a_0 \\ B(L) &= bL^m, \qquad L \geq a_0 \end{aligned} \tag{17}$$

The upper limit of integration was taken as infinity, although any large value would suffice since $B(L)$ decreases so rapidly with size. Thus, the nucleation rate is given by

$$B^0 = -\frac{b}{(m+1)}a_0^{m+1} \tag{18}$$

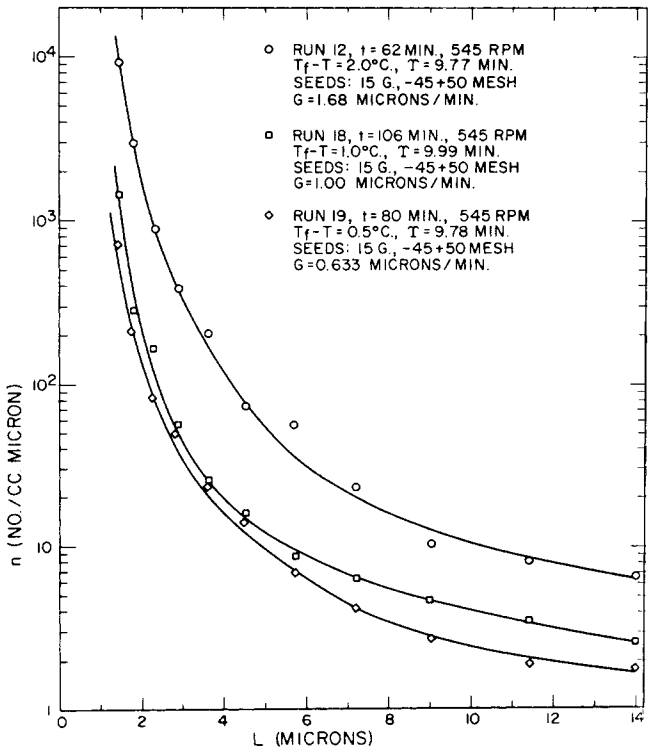

Fig. 3. Typical size distributions.

Several values of a_0 were used in subsequent correlations.

2. In the second method, the critical size a_0 was set equal to zero, and the birth function taken as

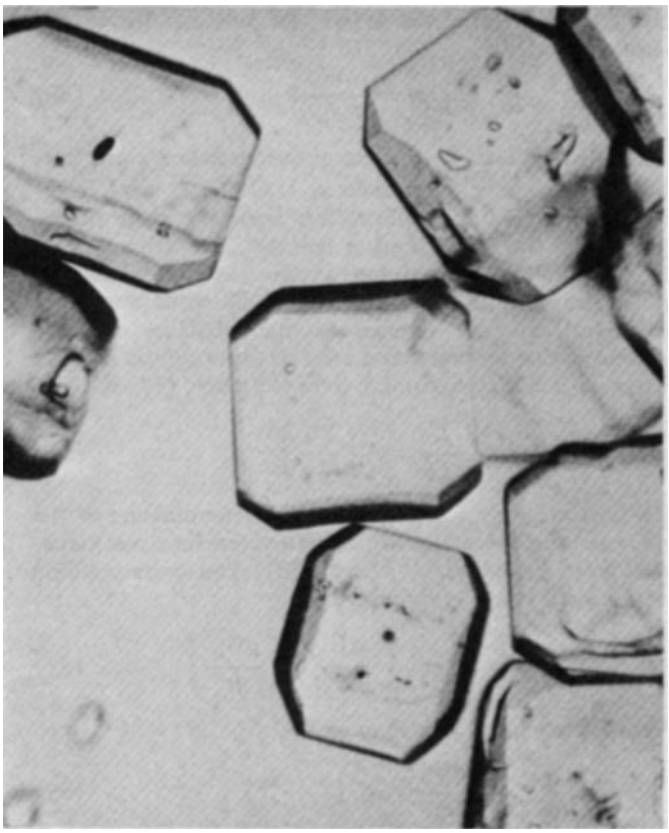

Fig. 4a. Photomicrograph of seed crystal run 15, $t = 94$ min., $G = 1.11$ microns/min., 545 rev./min.

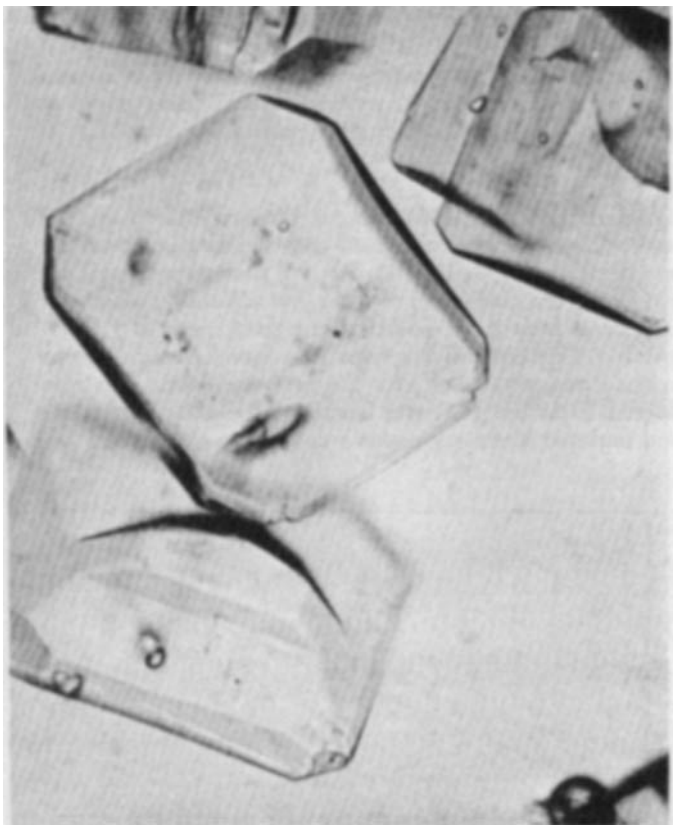

Fig. 4b. Photomicrograph of seed crystal run 15, $t = 207$ min., $G = 0.79$ microns/min., 610 rev./min.

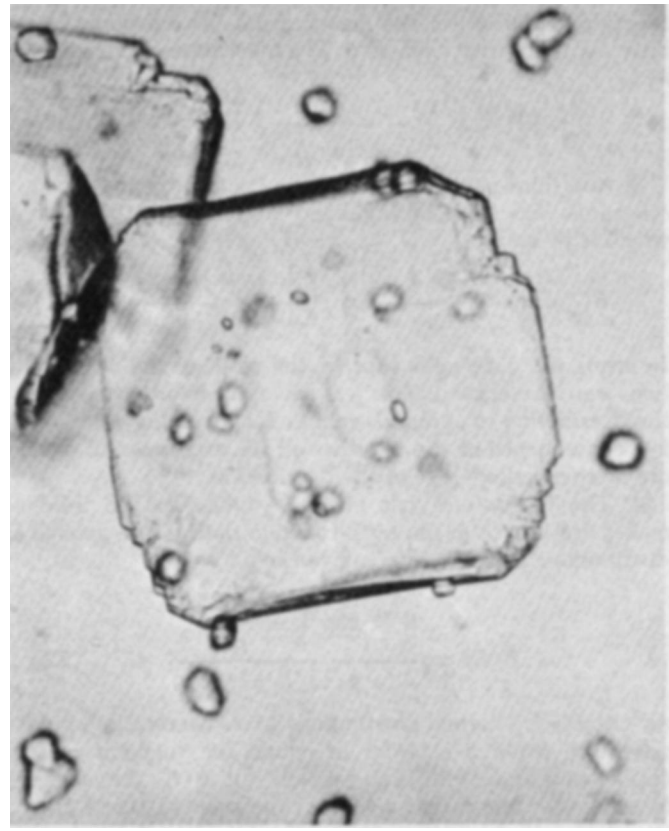

Fig. 4c. Photomicrograph of seed crystal run 15, $t = 298$ min., $G = 0.65$ microns/min., 675 rev./min.

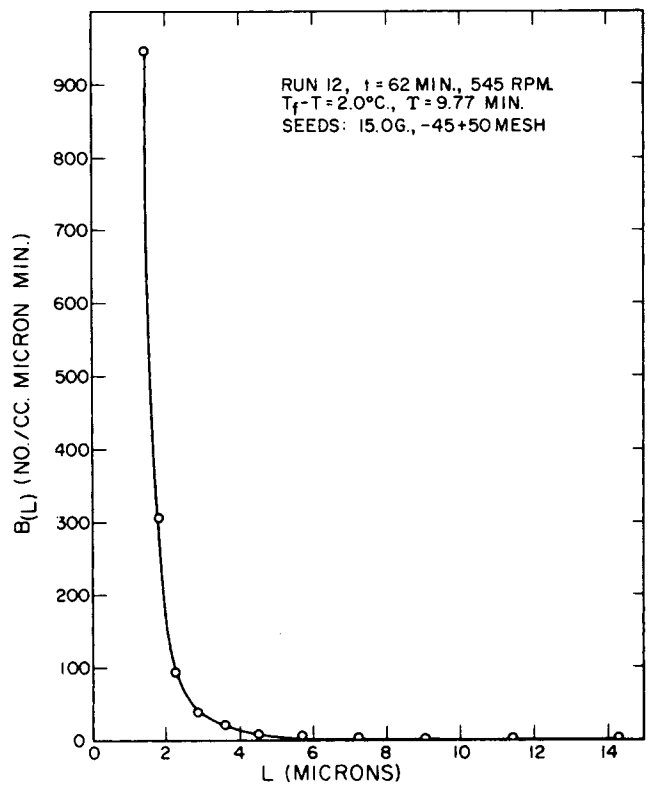

Fig. 5. Typical birth function.

$$B(L) = ba^{m-1}L \qquad L \leq a$$
$$B(L) = bL^m, \qquad L \geq a \tag{19}$$

The constants b and m were determined as before. The method is similar to that above, except that the birth function to the left of the maximum as "a" is assumed to be linear in L rather than zero. The nucleation rate is given by

$$B^0 = \left(\frac{1}{2} - \frac{1}{m+1}\right) ba^{m+1} \tag{20}$$

3. As a third method, the birth function in the measured size range was fit to the modified log normal distribution which is given by

$$B(L) = \frac{B^0}{\sqrt{2\pi}\log\sigma'} \exp\left[\frac{-\log^2(L/L')}{2\log^2\sigma'}\right] \tag{21}$$

In fitting the data, values for L', the mode of the distribution, were preselected. This was necessary in order to force the distribution to approach zero as L approaches zero and is a consequence of the fact that all the experimental data are on the leading edge of the distribution.

4. The fourth and last method, similar to the third, makes use of a fit of the birth function data to the gamma distribution. This function is given by

$$B(L) = \frac{B^0 L^\alpha \exp\left[-\frac{\alpha L}{\beta}\right]}{\Gamma(\alpha+1)(\beta/\alpha)^{\alpha+1}} \tag{22}$$

As with the log normal distribution, it was necessary to preselect the mode β in order to bound the function as L approaches zero. With each method, the $B(L)$ data were fit using only the 6 data points at the smallest sizes. This was done in order not to give undue weight to the data at large sizes which contribute negligibly to the magnitude of the nucleation rate.

Each of the above methods for estimating the nucleation rate is somewhat arbitrary in the absence of population density data at sizes less than 1.26 microns and in the lack of knowledge of the growth rate over the size range of measurement. To test the veracity of these methods, the nucleation rates were correlated with the variables characterizing the secondary environment of the system. The method giving the highest correlation coefficient was taken as most reliable. Past work has indicated that the rate of secondary nucleation is a function of temperature, supersaturation, seed moment, and agitation level. Because the experiments were conducted in a very narrow temperature range (33° to 34.5°C.), temperature was deleted as a correlating variable. Stirrer rev./min. was taken as an appropriate measure of agitation level. Since ammonium sulfate-water is a Class II system, there was no reliable direct method of determining supersaturation at the low levels which existed in the crystallizer. This made it necessary to employ the growth rate of the seed crystals as an indirect measure of supersaturation. This is reasonable, since crystal growth rates have generally been found to be proportional to low powers of supersaturation,

$$G = k_G S^\delta \tag{23}$$

with δ often lying between 1 and 2. The jth moment of the seed size distribution as given by

$$M_j = \left[\frac{N}{V_T}\right](\bar{L})^j \tag{24}$$

was taken as the correlating variable describing the effects of the seed bed. The number of seeds N was obtained from the initial seed mass, the initial seed size and the crystal density

$$N = \frac{W_i}{k_v L_i^3 \rho} \tag{25}$$

Since the length to width ratio of the seeds was close to 1, the shape factor k_v was taken as 1. G and $\bar{L}$ were determined by combining information from the seed photographs and the Class II mass balance. The average seed size at various times during a run was determined by measurement of the images of 10 to 20 seeds appearing in the photographs. To increase the reliability of these measurements, the measured seed size was correlated with the corresponding seed mass from Equation (6) using

$$\frac{\bar{L}}{L_i} = A\left[\frac{W_t}{W_i}\right]^B \tag{26}$$

The data are shown in Figure 6. For determination of the moments, the average seed size at a given time was calculated from Equations (6) and (26). The corresponding seed growth rate was found from

$$G = \frac{d\bar{L}}{dt} = \left[\frac{d\bar{L}}{dW_t}\right]\left[\frac{dW_t}{dt}\right] \tag{27}$$

From Equation (6), which gives W_t,

$$\frac{dW_t}{dt} = kQ(T_f - T) \tag{28}$$

and from Equation (26)

$$\frac{d\bar{L}}{dW_t} = B\frac{\bar{L}}{W} \tag{29}$$

Hence, the growth rate is given by

$$G = kQ(T_f - T)B\frac{\bar{L}}{W_t} \tag{30}$$

The nucleation rate data, which consisted of 67 points from eight different runs, were correlated using a power law model describing the dependence of the variables

$$B^0 = c_0\,(\text{rev./min.})^{c_1}\,(G)^{c_2}\,(M_j)^{c_3} \tag{31}$$

Although Equation (31) has no fundamental theoretical basis, this model has been used with some success in other investigations (*6, 9, 11, 13*). Each of the methods used for estimating the nucleation rate has one adjustable parameter associated with it. In addition, the seed moment j is adjustable. Consequently, a two dimensional search on the method parameter and j for the best correlation was conducted. Equation (31) was linearized by taking logarithms and multiple linear regression was used to obtain best val-

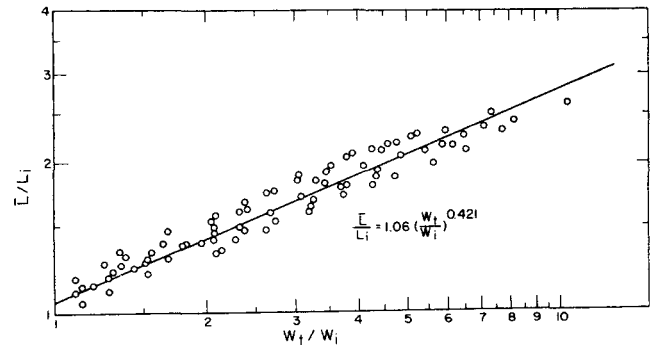

Fig. 6. Correlation of seed size with seed mass.

TABLE 1. CORRELATION COEFFICIENTS (R^2) FOR FIT OF B^0 DATA
($\overline{R}_1^2$ is the average for the fit of $B(L)$ data)

	Method 1			Method 2			Method 3			Method 4		
	$a_0 = 1.0$	$a_0 = 1.2$	$a_0 = 1.425$	$a = 1.0$	$a = 1.2$	$a = 1.425$	$L' = 0.2$	$L' = 0.5$	$L' = 1.0$	$\beta = 0.25$	$\beta = 0.5$	$\beta = 1.0$
	$\overline{R}_1^2 =$	$\overline{R}_1^2 =$	$\overline{R}_1^2 =$	$\overline{R}_1^2 =$	$\overline{R}_1^2 =$	$\overline{R}_1^2 =$	$\overline{R}_1^2 =$	$\overline{R}_1^2 =$	$\overline{R}_1^2 =$	$\overline{R}_1^2 =$	$\overline{R}_1^2 =$	$\overline{R}_1^2 =$
j	0.948	0.948	0.948	0.948	0.948	0.948	0.939	0.923	0.884	0.883	0.870	0.832
0	0.726	0.716	0.699	0.725	0.725	0.717	0.678	0.703	0.692	0.702	0.697	0.686
1	0.759	0.751	0.736	0.755	0.758	0.752	0.701	0.734	0.728	0.735	0.732	0.721
2	0.788	0.786	0.774	0.778	0.786	0.785	0.713	0.762	0.765	0.765	0.766	0.759
3	0.796	0.801	0.795	0.779	0.793	0.798	0.703	0.766	0.782	0.775	0.779	0.779
4	0.783	0.792	0.790	0.762	0.780	0.789	0.682	0.753	0.777	0.762	0.772	0.776
5	0.765	0.775	0.777	0.742	0.761	0.772	0.660	0.733	0.761	0.744	0.754	0.762

ues of c_0, c_1, c_2, and c_3. The quality of fit of the data was examined in terms of the square of the multiple correlation coefficient R^2. Table 1 summarizes these results. The best fit of the data was obtained using method 1 to evaluate the nucleation rate with $a_0 = 1.2$ microns and $j = 3$. Interestingly, this value of a_0 is essentially the lower size edge of the experimental population density data. Hence, the method which gives the best correlation of the nucleation rates is also the least arbitrary in the sense that only data in the measured size range are used to evaluate B^0. That the third moment appears in the best correlation indicates that the mass concentration of seeds is the proper correlating variable. Consequently, the nucleation rate data were recorrelated using the mass concentration calculated directly from the Class II mass balance and the slurry volume with the result

$$B^0 = 1.04 \times 10^{-18} \text{ (rev./min.)}^{7.84} G^{1.22} (M_T)^{0.98} \quad (32)$$

R^2 was improved slightly to 0.816. Figure 7 shows the predicted and experimental data.

DISCUSSION

The strong dependence of the nucleation rate on stirrer rev./min. and essentially first power dependence on solids concentration shown by Equation (32) coupled with the seed photographs of Figure 4 provide strong evidence that secondary nuclei are generated by collisions of the seed crystals with the impeller blades. These observations are consistent mechanistically with the work of Lal et al. (5), Clontz and McCabe (2), and Johnson et al. (4), who showed qualitatively that crystal-solid impacts induce nucleation. The very strong dependence on stirring rate is likely a consequence of two factors. First, increasing the stirring rate increases the frequency of seed collisions with the impeller. Secondly, the impact energy is greater at high stirring rates which provide high relative velocities between the impeller and the seed crystals. This interpretation is supported by Clontz and McCabe (2) who showed for $MgSO_4 \cdot 7H_2O$ that no nuclei were produced in the absence of crystal-solid contacts and that the number of nuclei resulting by impact of a glass rod was essentially linear with impact energy per unit area. Micro-attrition due to crystal-impeller collisions is further substantiated by the sequence of microphotographs shown in Figure 4. As stirrer rev./min. is increased in sequence, a marked progression of fissures and cracks develops at the corners of the seed crystals. At 545 rev./min. the seed crystals appear virtually free of visible surface flaws while at 675 rev./min. severe defects at the corners have developed. This is not to say that the micro-attrition mechanism is absent at the lower stirring rate. Rather, the rate of micro-attrition at high rev./min. exceeds the ability of the crystal surface to heal by growth. This effect was compounded by the lower growth rates occurring toward the end of the run, while rev./min. were stepped upward as the run progressed.

The observed dependence of the nucleation rate on seed crystal growth rate to the 1.22 power likely indicates at least 1.22 power dependence on supersaturation, a consequence of the fact that growth rates normally are at least linear with supersaturation. The dependence of secondary nucleation on supersaturation may be interpreted in various ways. As Clontz and McCabe suggest, the number of aggregates of solute molecules which are loosely held at a crystal surface and which may be dislodged by impacts probably increases with supersaturation. Also, the critical nucleus size is inversely proportional to supersaturation, so supersaturation may be a measure of the ability of nuclei to survive rather than redissolve. Another possible explanation is that supersaturation is a measure of the ability of seed crystals which have undergone attrition to heal and thus produce more nuclei. In addition, crystals which grow rapidly at high supersaturation levels generally have less mechanical strength than slow growing crystals and thus may be more susceptible to attrition.

Although definitive kinetic studies of secondary nucleation have been relatively infrequent, most have resulted in correlations of the type shown in Equations (31) and (32). Randolph and Cise (1, 9) studied secondary nuclea-

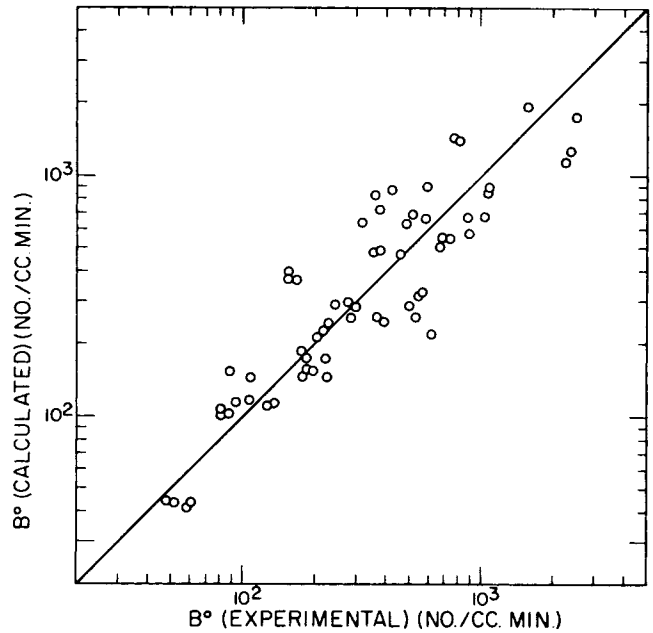

Fig. 7. Results of nucleation rate correlation.

tion of K_2SO_4 using the same equipment and essentially the same experimental techniques employed here as well as similar data analysis techniques. They found the nucleation rate to be proportional to approximately the 6th power of stirrer rev./min., the 0.6 power of supersaturation and the 4th moment of the seed size distribution. Timm and Larson (*13*), using MSMPR data, indicate that nucleation rate has 9th order dependence on supersaturation (as characterized by growth rate) for the system NaCl-EtOH-H_2O, 4th order for $(NH_4)_2SO_4$-MeOH-H_2O, and 1st order for alum-EtOH-H_2O. In a companion study, Larson et al. (*6*) showed the nucleation rate for the latter two systems to be linear with suspension density.

Heretofore, most data from MSMPR investigations have been analyzed successfully using Equation (10) which assumes that the size distribution is populated by growth of nuclei generated at essentially zero size. It appears that this success has been due at least in part to the fact that population densities have been determined for quite large sizes where growth is largely independent of size and where birth is truly negligible. If [as the results of the present study, those of Randolph and Cise (*9*) and the theory of Wey and Estrin (*14*) have indicated] the growth rates of very tiny crystals are small but increase rapidly with size, the nucleation rates obtained by extrapolation of MSMPR data to zero size may not be true nucleation rates. Rather, they would be effective rates which reflect only the number of nuclei which were large enough originally and remained in the crystallizer sufficiently long to grow to a size where the growth rate is large and constant. Large numbers of other nuclei may simply be washed out of the crystallizer and are ineffective in populating the large size ranges. Presuming this analysis to be correct, two features of MSMPR data are suggested. First, if the population density is measured at very small as well as large sizes, the slope of ln n versus L should be greater at small sizes than at large. This will be a consequence of lower growth rates at the small sizes and of the birth of nuclei. The data of Rosen and Hulburt (*11*) for the continuous vacuum crystallization of K_2SO_4 show precisely this behavior. Secondly, the effective nucleation rate should increase with increasing residence time, other factors such as stirring rate, supersaturation, etc. being equal. However, it is normally not possible to increase the residence time for an MSMPR crystallizer without also decreasing the supersaturation level. Depending on the extent to which these cancel each other in their effect on nucleation rate, the *apparent* dependence on supersaturation for the *effective* nucleation rate may be positive, negative, or zero. This likely is the reason that Rosen and Hulburt (*11*) and Larson and Genck (*3*) found essentially zero order dependence on supersaturation for the nucleation rate of K_2SO_4 using an MSMPR crystallizer while Randolph and Cise (*9*) found +0.6 order dependence. Rosen and Hulburt and Larson and Genck measured effective nucleation rates, while Randolph and Cise measured values closer to the true nucleation rate.

PREDICTION OF CSD

The kinetic expression for nucleation rate, Equation (32), can be used to predict particle size in an MSMPR crystallizer. Evaluating Equation (32) at the median rev./min. of 610 gives

$$B^0 = k_N' G^i M_T^j \tag{33}$$

where $i = 1.217$, $j = 0.98$, and $k_N' = 6.77 \times 10^3$. The solids concentration in a Class II MSMPR crystallizer is given as

$$M_T = \Delta C = 6\rho k_v B^0 G^3 \tau^4 \tag{34}$$

Substituting general power-law nucleation kinetics Equation (33) into the mass balance expression Equation (34) gives

$$G = \left[\frac{M_T^{1-j}}{6\rho k_v k_N' \tau^4}\right]^{\frac{1}{i+3}} \tag{35}$$

Thus, for the special case where nucleation rate is proportional to solids concentration, that is, $j = 1$, growth rate in a Class II MSMPR crystallizer is seen to be independent of feed concentration and depends only on retention time. Apparently, this is the case for ammonium sulfate. Multiplying Equation (35) by 3τ gives the predicted variation of dominant size with retention time for such a system. Thus

$$3G\tau = L_D = K\tau^{\left(1 - \frac{4}{i+3}\right)} \tag{36}$$

where

$$K = \left[\frac{3^{i+3}}{6\rho k_v k_N'}\right]^{1/(i+3)} \tag{37}$$

Evaluating the constants of Equation (37) using the kinetic constants for the ammonium sulfate system of the present study gives

$$L_D = 150\tau^{0.052} \text{ microns} \tag{38}$$

Thus, for a retention time of two hr. a dominant size of 193μ would be predicted. This value is lower than might reasonably be expected, indicating that indeed B^0 represents a maximum estimate of the nucleation rate. As discussed previously, most of the secondary nuclei are undoubtedly washed out of the system during their initial period of slow growth, leaving a much lower effective nucleation rate to populate the larger sizes observed as MSMPR product. Further, convective growth was suppressed in calculating B^0 and thus the values calculated represent a maximum estimate of secondary nucleation. Also, as discussed previously, the driving force dependence observed in these kinetics, namely $G^{1.22}$, might not be exactly reproduced in MSMPR data if the supersaturation dependence of the slow-growing nuclei differs from that of the macro-sized product. Thus, changes in supersaturation (brought about by changes in retention time) act differently on the nuclei and macro-sized crystals resulting in a variable washout of nuclei not predicted simply in terms of the retention time. The observed kinetic dependence of nucleation rate on solids concentration would probably be observed in MSMPR data. Dependence on stirrer rev./min. is much less certain since undoubtedly factors other than rev./min. are necessary in characterizing the effect of agitation. Unfortunately, no published MSMPR data for the ammonium sulfate system exist for comparison.

SUMMARY AND CONCLUSIONS

An apparatus described by Cise and Randolph (*1*) was used to study nucleation in the ammonium sulfate-water system. Ammonium sulfate-water is a Class II (high yield) system. Feed solution quickly adjusts to a concentration level close to the solubility value when backmixed in the presence of seed crystals. Even with no seeds present, only small supersaturations could be sustained without copious formation of nuclei which quickly grew to relieve the excess supersaturation. Such homogeneous nucleation could explain the tendency towards unstable CSD observed for the ammonium sulfate system.

Nucleation at low supersaturations in seeded solutions occurs by secondary mechanisms. Nuclei are formed by micro-attrition of seed crystals over the size range of measurement of this study, 1.26 to 25.4 microns. This is evidenced by the immediate response of the population densities for all sizes to a step change in rev./min. Strong dependence of nucleation rate on agitation rate and photomicrographs of the seed crystals also support this view.

Nucleation rates in the size range of measurement were determined from the birth distribution function $B(L)$. $B(L)$ was calculated from population density data by suppressing the growth term in the population balance. Although not zero, the growth rates of the secondary nuclei are much lower than the growth rates of large seed crystals in the same environment. By implication, growth rates for this system are strongly size-dependent at the small particle sizes of this study.

The birth function was represented by several analytical but empirical forms and the nucleation rate was obtained by integration. The relationship $B(L) = mL^b$ was found to best represent the data.

Nucleation rate was correlated with the characteristics of the secondary environment with the result

$$B^0 = 1.04 \times 10^{-18} \text{ (rev./min.)}^{7.84} (G)^{1.22} (M_T)^{0.98}$$

The arbitrariness in the definition of total nucleation rate as illustrated in this paper unfortunately limits the quantitative utility of these data in predicting CSD in other configurations. However, the factors influencing secondary nucleation are clearly discernible. A rigorous quantitative definition and use of such secondary nucleation kinetics must await quantitative separation of size-dependent growth rates and birth rates, $G(L)$ and $B(L)$ at the small sizes measured, quantitative correlation of such growth rates with overall driving forces in the system, and measurement of secondary nucleation to low enough sizes that the form of the $B(L)$ function can be ascertained. Ironically, the increased detail and accuracy of secondary nucleation measurements made in this study have indicated the near-impossibility of quantitatively characterizing secondary nucleation using the MSMPR technique as well as casting doubt on the general applicability of gross secondary nucleation kinetics so obtained.

ACKNOWLEDGMENT

The authors gratefully acknowledge the financial assistance provided by the National Science Foundation through Grant GK-10551.

NOTATION

a = constant in birth function correlation, method 2, microns
a_1 = largest size of nuclei, microns
a_0 = critical nucleus size, microns
A = constant in seed size-seed mass correlation
b = constant in birth function correlation, methods 1 and 2
B = constant in seed size-seed mass correlation
$B(L)$ = birth function, no./cc. micron
B^0 = nucleation rate, no./cc. min.
c_0, c_1, c_2, c_3 = constants in power law correlation of nucleation rate
C = solute concentration, g./cc.
C_f = feed concentration, g./cc.
C_s = concentration of saturated solution, g./cc.
$D(L)$ = death function, no./cc. micron
$G, G(L)$ = crystal growth rates, microns/min.
i = kinetic order of supersaturation in power model
j = kinetic order of solids concentration in power model
k = solubility constant, g./cc. °C.
k_G = crystal growth constant
k_n = nucleation rate constant
k_N' = nucleation rate constant
k_v = volume shape factor, dimensionless
L = crystal size, microns
L_D = dominant crystal size, microns
L_i = initial seed size, microns
$\overline{L}$ = mean seed size
m = constant in birth function correlation, method 1 and 2
M_j = jth moment of seed size distribution
M_T = solids concentration, g./cc.
n = population density, no./cc. micron
n_0 = population density at zero size, no./cc. micron
N = number of seeds
P = production rate, g./min.
Q_i = flow rate, cc./min.
S = supersaturation, g./cc.
t = time, min.
T = crystallizer temperature, °C.
T_f = saturation temperature of feed, °C.
V = crystallizer liquid volume, cc.
V_T = slurry volume, cc.
W_i = initial weight of seeds, g.
W_t = weight of seeds at time t, g.
α = constant in gamma distribution, dimensionless
β = mode of gamma distribution
δ = kinetic order of supersaturation in growth rate kinetics
σ' = coefficient of variation for log-normal distribution
ρ = crystal density, g./cc.
τ = residence time, min.

LITERATURE CITED

1. Cise, M. D., and A. D. Randolph, *Chem. Eng. Progr. Symp. Ser.*, to be published.
2. Clontz, N. A., and W. L. McCabe, Paper presented at 62nd Am. Inst. Chem. Engrs. Annual Meeting, Washington, D. C. (1969).
3. Genck, W. J., and M. A. Larson, Paper presented at 3rd Am. Inst. Chem. Engrs.-IMIQ Joint Meeting, Denver, Colorado (1970).
4. Johnson, R. T., R. W. Rousseau, and W. L. McCabe, *ibid.*
5. Lal, D. P., R. E. A. Mason, and R. F. Strickland-Constable, *J. Crystal Growth*, **5**, 1 (1969).
6. Larson, M. A., D. C. Timm, and P. R. Wolff, *AIChE J.*, **14**, 448 (1968).
7. Mason, R. E. A., and R. F. Strickland-Constable, *Trans. Faraday Soc.*, **62**, 455 (1966).
8. Randolph, A. D., *Can. J. Chem. Eng.*, **63**, 280 (1964).
9. ———, and M. D. Cise, paper submitted to *AIChE J.*
10. Robinson, J. N., and J. E. Roberts, *Can. J. Chem. Eng.*, **56**, 105 (1957).
11. Rosen, H. N., and H. M. Hulburt, Paper presented at 62nd Am. Inst. Chem. Engrs. Annual Meeting, Washington, D. C. (1969).
12. Sherwin, M. B., R. Shinnar, and S. Katz, *AIChE J.*, **13**, 1141 (1967).
13. Timm, D. C., and M. A. Larson, *AIChE J.*, **14**, 452 (1968).
14. Wey, J. S., and J. Estrin, *Chem. Eng. Progr. Symp. Ser.*, to be published.

Manuscript received June 21, 1971; revision received November 30, 1971; paper accepted December 5, 1971.